

Chapter 12

Biopatterns Created Using Colloidal Templates

Qin Li, Maria Askildsen and Ehsan Eftekhari

12.1 Introduction

Colloids refer to particles in the size range of a few nanometres to a few micrometres. When the colloidal particles are monodispersed in size, upon favourable conditions, they can spontaneously assemble into ordered assemblies, named ‘colloidal crystals’. Colloidal assemblies can be either two-dimensional (2D) or three-dimensional (3D) periodically structured lattices, and they serve as excellent templates for patterning [1]. Colloidal templating is also sometimes referred to as colloidal lithography. 2D hexagonal lattices of colloidal spheres have been successfully demonstrated as physical masks for fabrications of ordered arrays of micro- or nanostructures, whilst 3D colloidal crystals have often been employed as removable templates for highly ordered, macroporous materials with partial photonic bandgaps, which have applications in sensors and optoelectronic devices [2]. In colloidal templating, the most commonly used colloidal particles are either polystyrene (PS) spheres or silica spheres, owing to the well-established synthesis methods for controlling particle size with tight monodispersity and the ease in removal as a template [2].

Colloidal templating is a very versatile technique; the 2D and 3D colloidal crystals can serve as templates for depositing various metals, catalysts, polymers and inorganic materials and forming inversed replica structures [3–6]. Colloidal templating has salient advantages in that it does not require any elaborate lithography equipment, it is intrinsically a parallel process and can be easily integrated with existing material deposition techniques such as sputtering/evaporation [7], chemical

Q. Li (✉) · M. Askildsen

School of Engineering (Environmental), Griffith University, Nathan, QLD 4111, Australia
e-mail: qin.li@griffith.edu.au

Queensland Micro- and Nanotechnology Centre, Griffith University,
Nathan, QLD 4111, Australia

E. Eftekhari

Queensland Micro- and Nanotechnology Center and School of Engineering, Griffith University,
170 Kessels Rd, 4111 Nathan, QLD, Australia
e-mail: ehsan.eftekhari@griffithuni.edu.au

© Springer International Publishing Switzerland 2015

J. Rodríguez-Hernández, A. L. Cortajarena (eds.), *Design of Polymeric Platforms for Selective Biorecognition*, DOI 10.1007/978-3-319-17061-9_12

325

vapour deposition [8], reactive ion etching [9], plasma treatment [10] and inkjet printing [11] to produce patterns of desired chemistry.

Self-assembled colloidal templates have been used to successfully pattern and culture cellular structures such as bacteria [12], and human cell cultures [13, 14] by providing an underlying protein pattern. The morphology and growth direction of biological microstructures can also be controlled by the substrate topography—both natural, and synthesized (e.g. fabricated nanostructures)—and is a major area of research in tissue engineering such as scaffold design for regenerative therapies [15]. In those patterning formats, the colloidal assembly can be used either as the direct underlying surface, or a sacrificial template. The formed patterns can be either disconnected or interconnected. Ordered patterns imply uniformity and optimum density, and they are compatible with array systems, and signal read-out platforms. Colloidal crystals also possess special optical features originated from Bragg's diffraction owing to their structural periodicity, which may be exploited particularly in sensing technologies. Moreover, colloidal self-assembly can be combined with supramolecular chemistry [16] or soft lithography [17] for creating hierarchical patterning.

The patterns generated by colloidal templating can be controlled in the range from several nanometres to several micrometres. When the pattern feature size is two or three orders of magnitude larger than proteins themselves, the protein adsorption behaviour is not different from protein adsorption on a non-patterned surface with the same surface chemistry, governed by the same fundamental protein–surface interactions, such as physisorption, chemisorption and bioaffinity. But when the pattern dimensions become comparable to the protein size, the protein–surface interaction can become atypical, which deserves particular attention [18]. We should also be mindful of that, proteins are delicate biomolecules which are prone to denaturation if chemically treated, and this critical factor must be considered when selecting or developing a patterning strategy.

This chapter intends to provide an overview on protein patterning generated by colloidal templating including the fabrications, properties and their applications. It aims to serve as a compendium for researchers and industry readers who are interested in this technology.

12.2 Fabrications of Colloidal Crystal Templates

Since the colloidal templates are the basis for this technology, we first introduce the fabrication methodologies for producing the 2D, 3D and hierarchically ordered colloidal crystals.

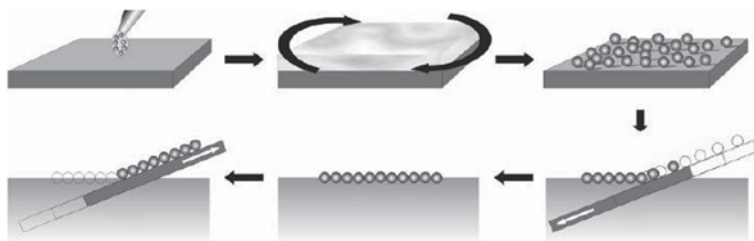


Fig. 12.1 Monolayer formation at the air–water interface from a spin-coated parent substrate by the SC method [23]

12.2.1 2D Colloidal Crystals

12.2.1.1 2D Close Packing

Self-assembling of 2D colloidal crystals (also *colloidal monolayers*) often involves a solvent drying process and an air–water interface; it is highly dependent on the interplay between the capillary forces and DLVO force among the colloidal particles [19]. The fabrication of 2D colloidal crystals can be categorized into two main approaches: (1) direct assembly on targeted substrate materials, or (2) pre-assembly on an intermediate surface, typically at air–water interface, with subsequent transfer onto the target. In the former case, the monolayer is created by either drying a colloidal suspension on a very smooth substrate such as mercury or by vertical lifting deposition [20, 21] or spin coating [22].

Retsch et al. [23] developed a more reproducible method whereby close-packed colloidal 2D crystals were constructed through floatation and re-deposition of PS particles at the air–water interface. As depicted in Fig. 12.1, in this method, a PS colloidal dispersion is first spin-coated onto a solid support termed the ‘parent substrate’ in a sparsely distributed fashion. After the dispersion is dried, the parent substrate is slowly immersed at a shallow angle in MilliQ water with moderate addition of sodium dodecylsulfate surfactant and/or pH-adjustment, causing the colloidal particles to detach and float at the air–water interface. The detached particles spontaneously self-assemble into a dense monolayer and remain afloat at the interface. A second ‘receiving substrate’ is then immersed into the water and slowly withdrawn at a shallow angle and collects the floating colloidal monolayer.

The method can produce high quality 2D colloidal crystals with large domain size spanning hundreds of micrometres as shown in Fig. 12.2. Moreover, the 2D assemblies exhibit strong mechanical stability; they can be transferred onto curved receiving surfaces, such as on tubular surface and undulating surfaces such as the ones formed by 2D crystals of different particle sizes as shown in the right panel in Fig. 12.2 [23].

The additional advantage of the method is that the 2D colloidal crystals formed at the air–water interface can be transferred onto both hydrophilic and hydrophobic

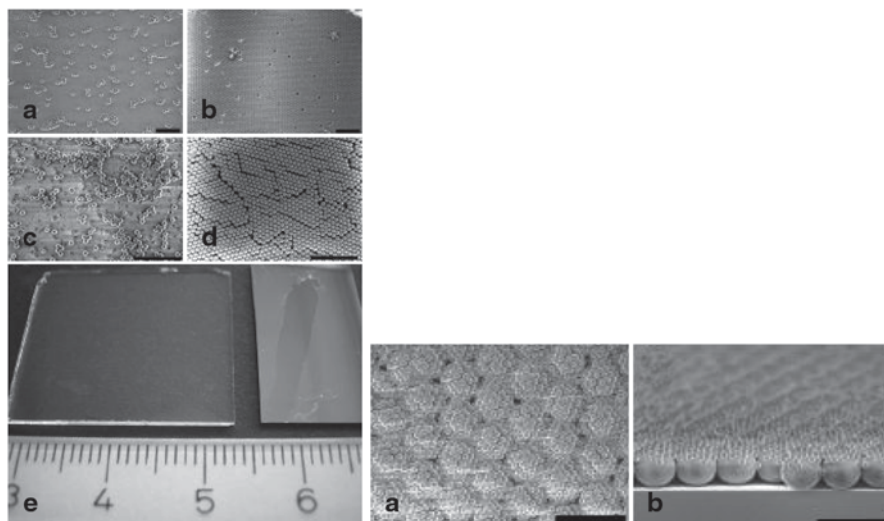


Fig. 12.2 *Left panel:* Formation of highly ordered, hexagonally close-packed monolayers (**b** and **d**) by floatation of sparsely distributed colloids of 1116 (**a**) and 182 nm (**c**), respectively. **e** shows a comparison of the 182 nm particles distribution on the parent substrate (*left*) versus a resultant close packed monolayer after floating (*right, dark grey patch*). *Scale bars* are 10 μm for **a** and **b**, and 2 μm for **c** and **d**. *Right panel:* stacking of PS monolayers of different particle size [23]

surfaces, as shown in the schematics in Fig. 12.3. This significantly enhances the versatility of this facile method.

12.2.1.2 Non-close 2D Ordered Packing

Non-close packed 2D arrays provide further flexibility in controlling pattern size, shape and inter-distance. Strategies have been developed to overcome the predestined hexagonal close packing structure governed by the thermodynamics. Zhou et al. [24] have invented a layer by layer method to produce non-close 2D

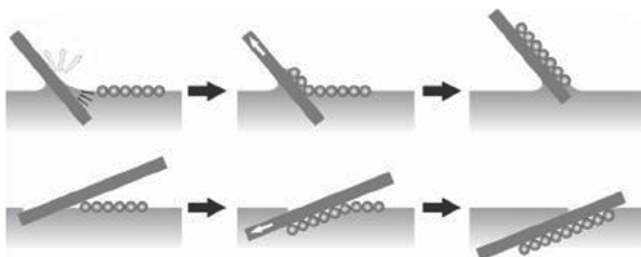


Fig. 12.3 Scheme: Transfer of a floating monolayer onto a hydrophilic (*top row*) and hydrophobic (*bottom row*) substrate

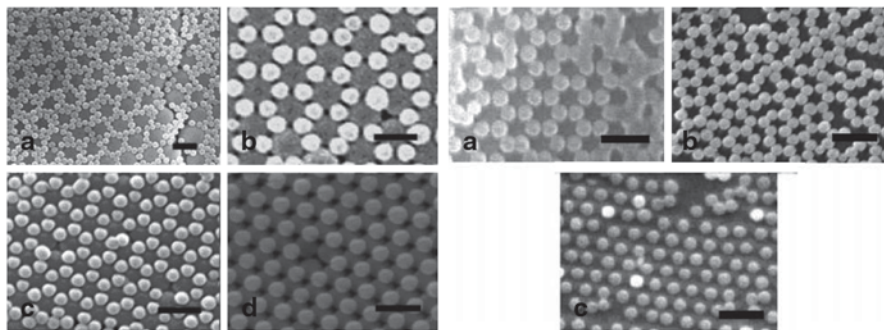


Fig. 12.4 *Left panel:* Silica monolayer patterns fabricated on PS colloidal films with size ratios of 0.28 (a), 0.4 (b), 0.48 (c) and 0.68 (d); *Right panel:* Remaining silica monolayer after removing the underlying PS colloidal films with size ratios of 0.4 (a), 0.48 (b) and 0.68 (c). The scale bar indicates 1 μm in all images [24]

packing, whereby a PS colloidal monolayer is first deposited on a glass substrate, followed by a second silica sphere layer deposited by vertical deposition, and subsequently heat treatment to remove the bottom PS layer. Figure 12.4 displays the SEM images of the structures after the bilayer formation and the following heat treatment.

Non-close packed 2D arrays can also be obtained by shrinking the size of colloidal spheres of the 2D hexagonal close packing. Vogel et al. [25, 26] have demonstrated that non-close packed 2D arrays can be used in combination with plasma etching to form the non-close 2D ordered packing. In their study, the non-close 2D packing enabled an inclined Au sputtering process to create novel nanostructures such as arrays of gold crescents, which showed heightened sensitivity in biosensing due to enhanced plasmonic effect.

12.2.1.3 2D Binary Colloidal Crystals

Singh et al. [27] have recently successfully fabricated 2D binary colloidal crystals with the two sizes of particles truly on the same plane. A modified Denkov 2D colloidal crystallization [28] was developed, whereby the colloidal solution of multicomponent colloids was confined inside a rubber ring placed on a hydrophilic surface to grow [10]. The schematic in Fig. 12.5 demonstrates the versatility of this binary colloidal monolayer in changing the chemical pattern geometry by using different composite binary colloidal assemblies (BCAs) as lithographic masks, and they can be utilized to adsorb proteins selectively after surface modification. Different chemical, micro- and nanopatterns can be created by exposing the templates to sputter-coating processes. Gold sputtering was chiefly employed in this study owing to its good compatibility with biomolecules.

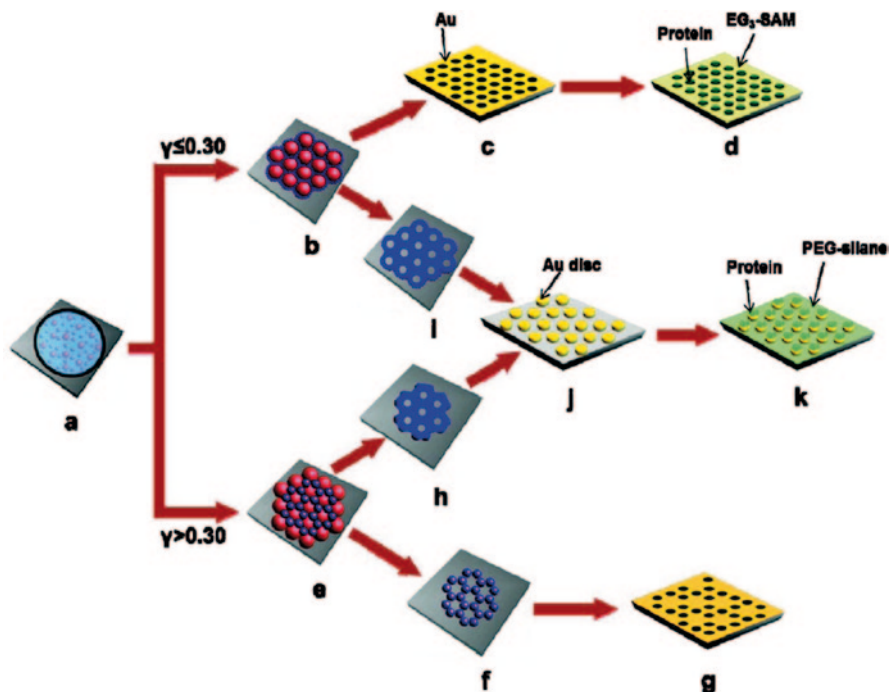


Fig. 12.5 Schematic illustration showing the generation of different chemical patterns from low and high size ratio BCAs, and subsequent protein patterning after surface modification of the patterned surface. **a** A mixed suspension of different sizes of colloidal particles is spread inside a rubber ring. **b, e** BCAs form after complete evaporation of the solvent. **c** Au sputtering over the colloidal mast and the removal of particles by sonication or lift-off yield chemically patterned surfaces. **f** Heating the composite template made from PS and SiO₂ particles for 5–10 min at 100°C and removal of SiO₂ particles by H. **g** Au deposition over the mast generates a chemical pattern comprising six holes arranged in hexagonal fashion. **h, i** Heating the composite masks for longer duration (20–45 min) at 120°C and removal of silica particles by HF. **j** Au deposition and subsequent removal of PS particles yield disk-like gold patterns. **d, k** The chemical modification of the patterned surface with protein resistant molecules guides the specific adsorption of the protein to unmodified regions [27]

12.2.1.4 Other Unconventional Patterns

The growth of thin film colloidal crystals can be influenced by substrate patterning. Key parameters influencing crystal formation include confining cell thickness, and the surface profile of the patterned substrate. Using the corrugated surface of commercially-available recordable DVDs as a wedge cell template, Ramiro-Manzano, Bonet [29] studied the growth of PS colloidal crystals. The researchers found that groove size, substrate pitch, cell thickness value and particle-to-substrate relative size dictated the deposited crystal configuration. For particles with size in order of the groove width, increasing cell thickness resulted in spherical particle distribution going from linear rows (i.e. reported ‘zigzag angle of 180 degrees’) to 60 degrees ‘zigzag’, and eventually to triangular arrangement of close-packed spheres as more

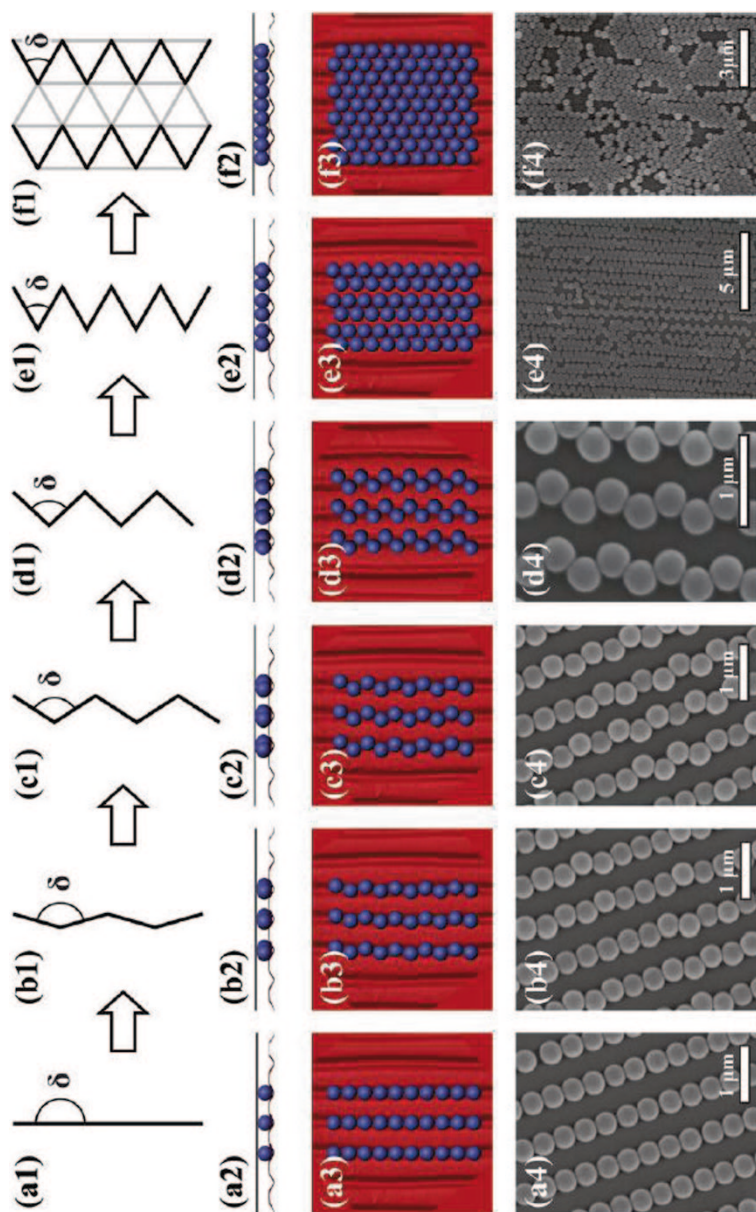


Fig. 12.6 SEM images (*bottom row*) of different particle orderings, the cell thickness increasing from the *left* to the *right* side of the panel. Side (*second row*) and top (*third row*) views of the ordering model showing the sphere distribution in the grooves. The *first row* shows how the zigzag angle of particle strips changes from 180° (**a**) to 60° (**e**). **f** A triangular arrangement of close-packed spheres. The particle size is 380 nm [29]

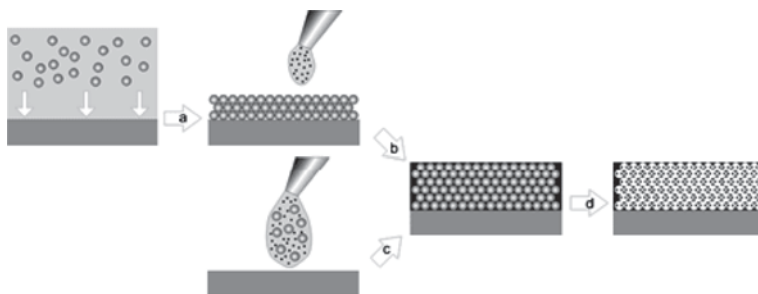


Fig. 12.7 Scheme of general preparation routes to 3D macroporous networks by colloidal crystal templating [32]

spheres are spatially accommodated and filling fraction is maximized (Fig. 12.6). When spherical particles of diameters larger than the corrugated groove width were used, the patterned surface could still influence particle ordering with a transitioning sequence of buckling, triangular and HCP observed—similar to that reported in non-patterned wedge cells. While localized dislocations and defects occurred, long-range patterning was essentially maintained [29]. The principles and techniques explored therefore provide opportunities to create large domain colloidal crystal arrangements of varying configurations based on tailored substrate structures using different colloidal particle sizes for applications where large surfaces areas or functional sites are required.

12.2.2 3D Colloidal Crystals

In comparison, the formation of 3D colloidal crystals is more straightforward and can be facilitated by a rich variety of methods, such as sedimentation in a force field, packing in a confined space, controlled evaporation including vertical lifting deposition [30] and horizontal deposition [31]. The most common type of colloidal crystals formed by self-assembly of monodisperse particles has a face-centred cubic (*fcc*) lattice symmetry with the highest crystalline packing density of 74% volume filling. Various operational parameters can be tuned in each process for controlling the film thickness.

3D colloidal crystals are often employed as templates for 3D macroporous networks. It is typically achieved by infiltrating the targeted precursor material into the interstitial voids of the colloidal crystal template, followed by solidification and subsequent template removal. The contact points between templating particles lead to orifices between the spherical voids in the resulting replica and consequently results in an open, fully continuous 3D network, often referred to as ‘inverse opals’.

The inverse opals can be formed in two principal ways, as illustrated in Fig. 12.7 [32]:

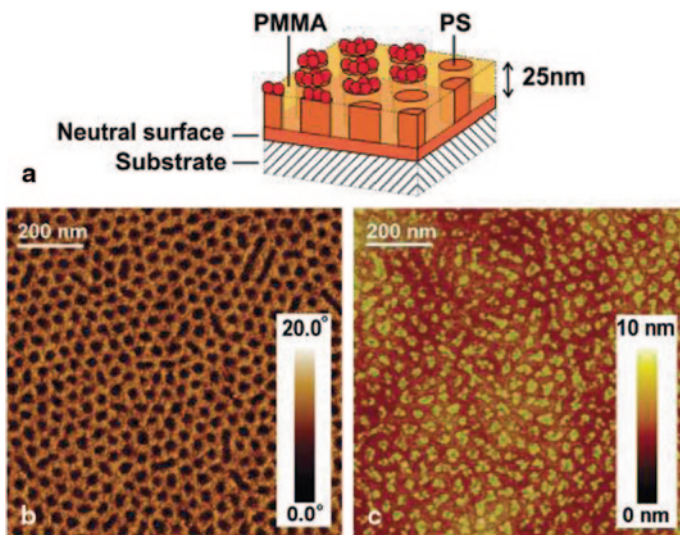


Fig. 12.8 **a** Schematic drawing of the PS-*b*-PMMA pattern on a neutral surface with proteins adsorbed on the PS domains. **b** AFM phase image showing the PS-PMMA ordered pattern. **c** AFM topography image showing that the IgG proteins are selectively adsorbed on the PS domains [34, 35]

- Infiltration with a second material, which can be polymer precursors, or sol-gel precursors, or a dispersion of nanoparticles, into the interstices of the colloidal template, followed by polymerization, solidification and template removal;
- Codeposition of the colloidal templates together with the matrix material, typically in the form of nanoparticles, followed by template removal.

12.2.3 Hierarchically Ordered Colloidal Crystals (HOCCs)

HOCCs are self-organized structures combining features of several hierarchical ordering characteristic length scales. Yang et al. [17] have first demonstrated this concept by combining copolymer templating (~ 10 nm), latex sphere templating (~ 100 nm) and micromolding ($\sim \mu\text{m}$) for the fabrication of hierarchically ordered porous oxides. HOCCs offer great potential for the design of new materials and devices for a broad range of applications due to the interconnected pores at different length scales, increased specific surface area, higher density of reactive sites and simultaneous patterning on surface [16].

Taking the colloidal particle size as the reference point, the larger length scale features can be conveniently introduced by incorporating mature microfabrication techniques, such as soft lithography through PDMS stamping, or photolithography, or silane chemistry combined with photolithography, whereas novelties often emerge from the pursuit of introducing additional features on the nanoscale. The

meso- and micro-size features can be introduced by surfactants, amphiphilic block copolymers, multi-size colloidal particles, anisotropic colloidal particles, ionic liquids and pre-functionalized constituent particles. Here we highlight the block copolymer co-assembly and multi-size colloidal particles co-assembly, due to their close pertinence to protein patterning. A more comprehensive account on HOCCs can be found in [33].

a. Block copolymer surface templating

Among those nanoscopic patterning methods, block copolymers is particularly relevant to protein patterning, because the phase separation as a result of the copolymer self-assembly can induce regular patterns that would have contrast in affinity to proteins or protein linker molecules [34, 35]. For example, polystyrene-*b*-poly(methyl methacrylate) can form cylindrical patterns with a PS domain size of tens of nanometres, which would favour protein adsorption, as shown in Fig. 12.8.

Fu et al. have introduced PS-*b*-PMMA copolymer in silica inverse opals using solution wetting [36]. Different from the previous studies, they succeeded in inducing the copolymer self-assembly along the inner surface of the inverse opal structure, instead of filling the pore volumes. The study showed a unique behaviour of copolymer self-assembly on a highly curved spherical surface with significant boundary constraints.

The study showed that the coexistence of polymer/silica and polymer/vacuum interfaces in the shells of the hollow spheres plays a synergetic role in block copolymer patterning, which can be adjusted by changing the commensurability between the block copolymer period and the shell geometry. Due to the confinement effect, the geometry and feature size of the copolymer patterns can be tuned by the pore size of the inverse opal as well as the molecular size of the copolymer, as demonstrated by their SEM images and the cartoon schematics in Fig. 12.9 They further demonstrated a hierarchical patterning of gold and palladium nanoparticles in the PS-*b*-poly(2 vinylpyridine) copolymer coated silica opal as shown in Fig. 12.9.

b. Multiple-size particle templating

Binary colloidal crystal (bCC) structures form when two species of colloidal particles in dispersion co-crystallize. Earlier fabrication processes of bCC structures were based on layer-by-layer deposition methods where a monolayer is initially prepared and subsequent monolayers are deposited on top containing different sized spheres. The resulting arrangement is that of stacked 2D monolayers, rather than a complete 3D binary structure.

An alternative approach to bCC fabrication was achieved by Wang et al. [37] using a simplified vertical lifting co-deposition method under thermodynamically non-equilibrium conditions. In this method, a mixed colloidal suspension is deposited onto a solid lifting support by vertical lifting action. Co-crystallization of large and small particles occurs due to kinetically controlled liquid flux-induced particle packing [37]. In the study, two experimental parameters were varied and their effect explored—(1) the size ratio of particles, $\gamma_{S/L}$ and (2) the relative concentration, $\phi_{S/L}$, where the subscripts S and L denote the small and large particles, respectively. The

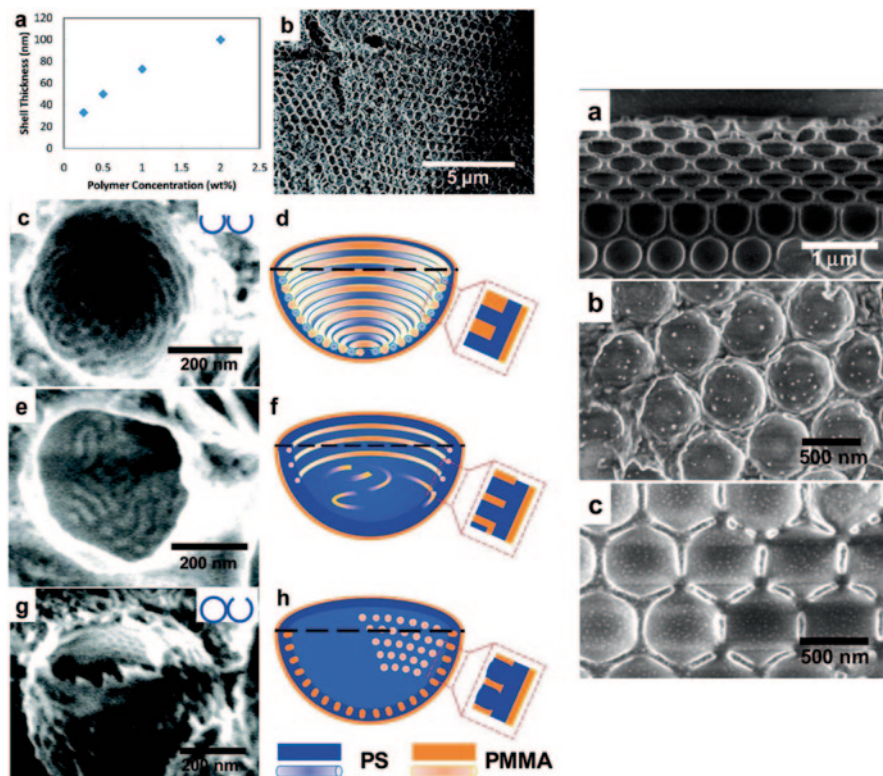


Fig. 12.9 *Left panel:* **a** Concentration dependence of shell thickness and the SEM images of, after removal of silica templates, **b** the 3D arrays of hollow PS-*b*-PMMA spheres and the annealed hollow spheres of **c** S_{326} -PMMA301, **e** S_{450} -MMA182 and **g** S_{1037} -MMA322. The PS-rich domains appear bright and the PMMA-rich domains appear dark in the SEM images. The schemes in **d**, **f** and **h** represent the schematic cross-section view of the nanostructured shells observed in **c**, **e** and **g**. *Right panel:* SEM images of Au/PS-P2VP hemisphere array with silica templates (side view) (**a**); before (**b**) and after annealing at 200°C for 24 h and with subsequent removal of silica templates (**c**)

lattice geometry commonly formed was found to be the close-packed face-centred cubic lattice (fcc) with tetrahedral or octahedral interstitial sites as illustrated in the schematic shown in Fig. 12.10. Figure 12.10 also presents the morphology of the 3D binary colloidal crystals when size ratio and relative concentration were varied.

The deposition method was simplified by Wang et al. [38] by a horizontal deposition method as illustrated by the schematic in Fig. 12.11. It was found that in horizontal deposition, the evaporation-induced liquid flux is fast enough to move the homogeneously distributed binary colloids to the drying edge without allowing them to segregate, thereby forming uniform binary crystal structures.

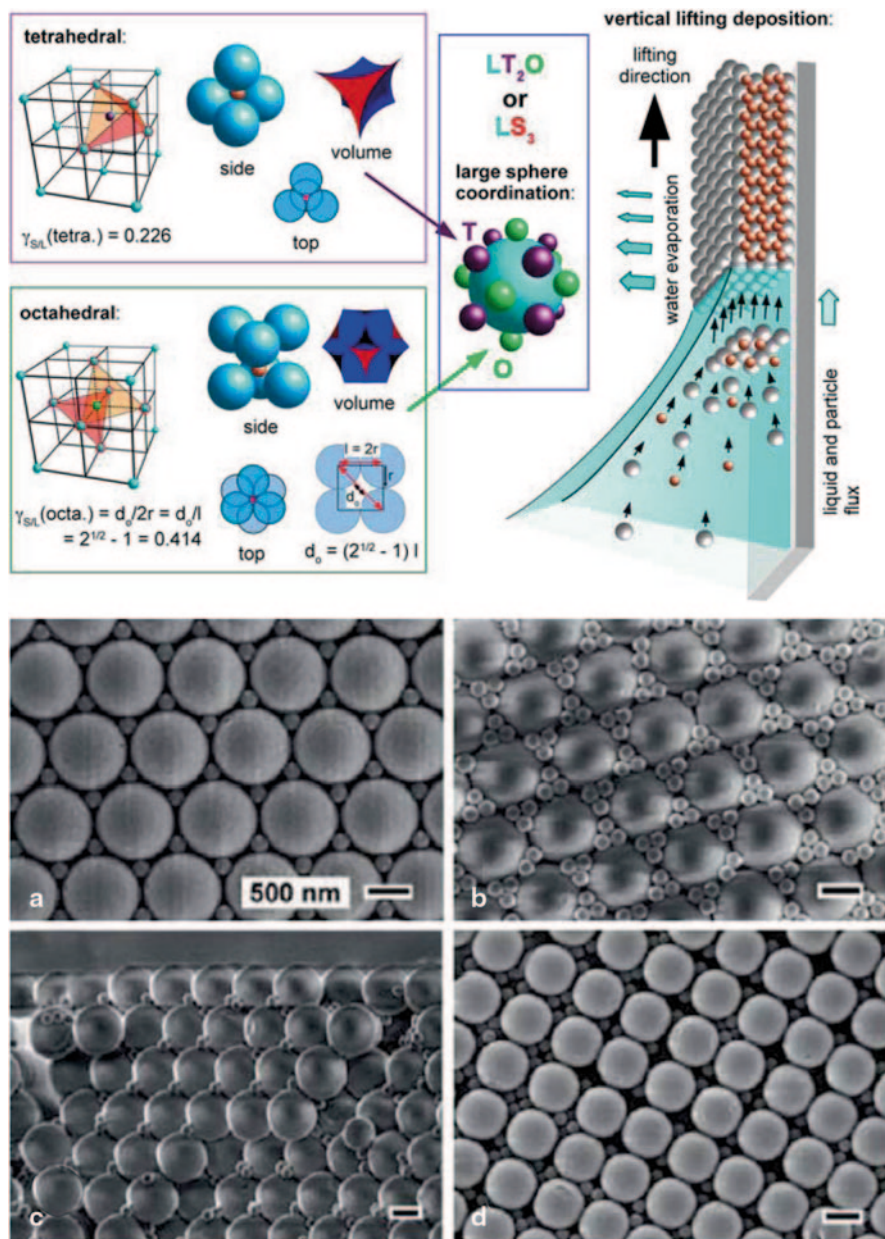


Fig. 12.10 *Left Panel:* Left: analysis of the fcc lattice geometry of large particles in blue with interstitial sites (tetrahedral in purple, left-top and octahedral in green, left-bottom) for accommodation of small particles. Right: schematic representation of the particle transfer and crystallization mechanism during vertical lifting deposition. *Right panel:* Top view onto a binary colloidal crystal of large ($dL=839$ nm, $\phi L=0.01$) and small ($dS=187$ nm, $\phi S=2.0 \times 10^{-4}$) with $\gamma S/L=0.223$, NS/NL=1.80. **b** Concentration of small particles $\phi S=3.84 \times 10^{-4}$, NS/NL=3.43. **c** Side view of a fracture through **a**. **d** Region with a square lattice geometry at small particle concentration of $\phi S=3.07 \times 10^{-4}$, NS/NL=2.77

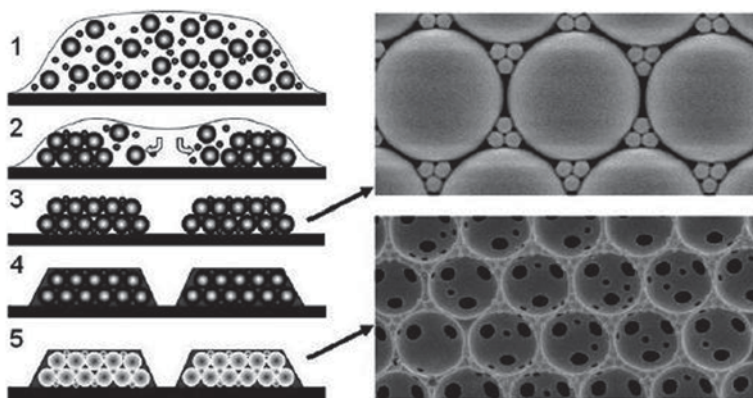


Fig. 12.11 Horizontal deposition method for fabrications of HOCCs

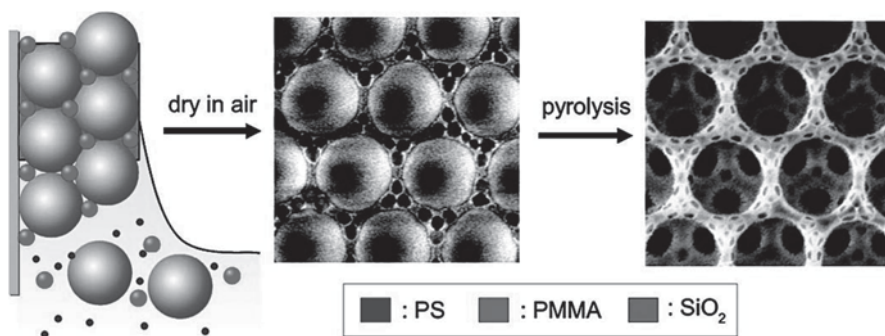


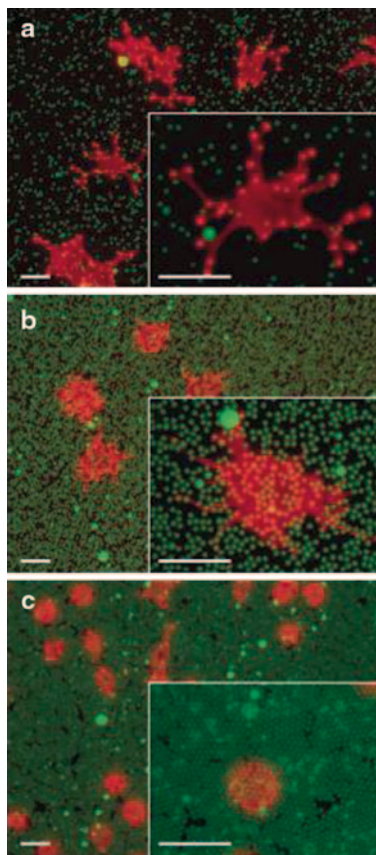
Fig. 12.12 Schematic and SEM image of multiple-size particle templating of hierarchically ordered binary colloidal particles [39]

Wang et al. [39] further demonstrated another important extension of this methodology, whereby they mixed three different types of colloids which are also of different size, namely 489 nm PS particles, 80 nm PMMA spheres and 12 nm silica nanoparticles. By a single stroke of vertical deposition, the three constituents co-crystallized into colloidal crystal formation, which is dominated by the large particle-induced periodicity with intermediate and small size particles filling the interstitial voids in an ordered fashion, as shown in Fig. 12.12.

12.2.4 Template Removal

In most cases in colloidal templating, the colloidal templates need to be removed after the desired patterns are formed. In 2D colloidal templating, the most frequently used method is the physical lift-off approach, which can be simply assisted by a piece of scotch tape. For 3D colloidal templating, particularly in inverse opal

Fig. 12.13 Spreading and morphology of fibroblast cells on different densities of colloidal particles. Fibroblasts attached and spread on particles presenting immobilized FN (*green*). Actin filaments in the cells were stained with rhodamine-phalloidin (*red*). Cell morphologies differ with particle organization. **a** Array with a sparse distribution of particles, 10.2% surface coverage, 2.19 μ particle spacing. **b** Array of intermediate density, 42.5% coverage, 0.59 μ particle spacing. **c** Close-packed array of particles, 96.5% coverage. All scale bars are 25 μ m



formation, the templates can be selectively removed by solvents, e.g. HF or NaOH solutions for removing silica colloids and toluene, tetrahydrofuran (THF) for removing PS colloids, or by heat treatment for removing the organic phase.

12.3 Protein Patterning Generated by Colloidal Templating

12.3.1 2D Patterning

12.3.1.1 Self-Assembly of Protein Coated Colloids

Carbeck and co-workers [14] have presented a straightforward approach to employ colloidal templating for patterning proteins. They used the streptavidin–biotin linking strategy to coat streptavidin-functionalized colloids with adhesion protein

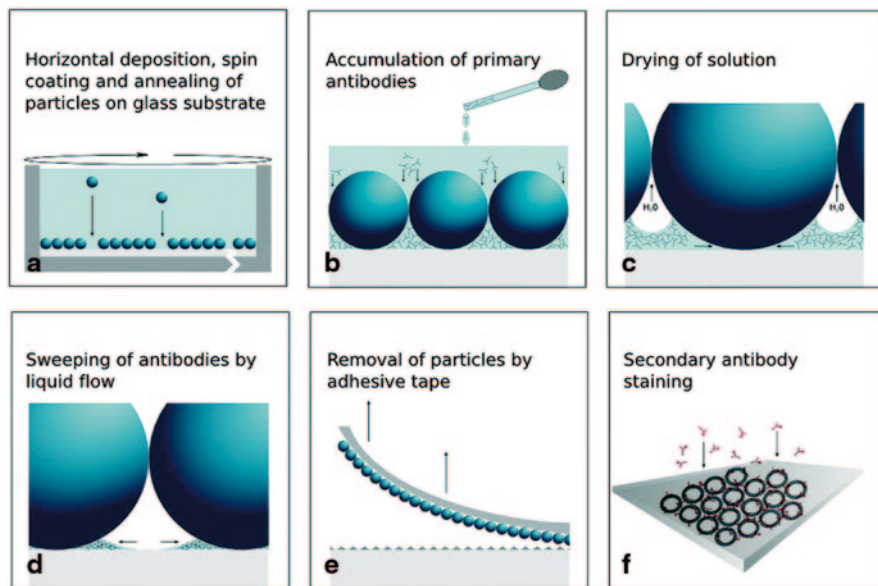


Fig. 12.14 Schematic drawing details the key steps in fabricating the protein annuli arrays [40]

fibronectin (FN) conjugated with biotin, followed by assembling the FN-coated colloids into 2D array by an electric-field assisted deposition. They then cultured fibroblast cells on colloidal arrays of different densities and used such a colloidal-templated protein patterns to study the biophysics underlying cell growth as shown in Fig. 12.13. They have demonstrated that colloidal assembly can control the composition of biomolecules on three different length scales, namely the size of individual particles, the spacing between particles and the length scale of the patterned area on a substrate.

12.3.1.2 2D Array Patterning

For developing biosensors for high-throughput protein and pathogen screening technologies, annulus-shaped protein structures are highly interesting, because the well-like structure comprised of protein is likely to enhance protein–protein interactions, thereby improve the detection sensitivity to antigens. Wolf and Li [40] have combined colloidal templating with drying lithography [41] and produced large-scale ($\sim\text{cm}^2$) 2D arrays of antibodies against *Escherichia coli* K12 and enhanced green fluorescent protein (eGFP) on versatile glass surfaces.

As illustrated by the Schematic in Fig. 12.14, the steps for generating this antibody annuli array include (a). 2D colloidal crystal template formation; (b). applying antibody solution (in PBS); (c). bulk solution drying; (d). sphere-substrate contact

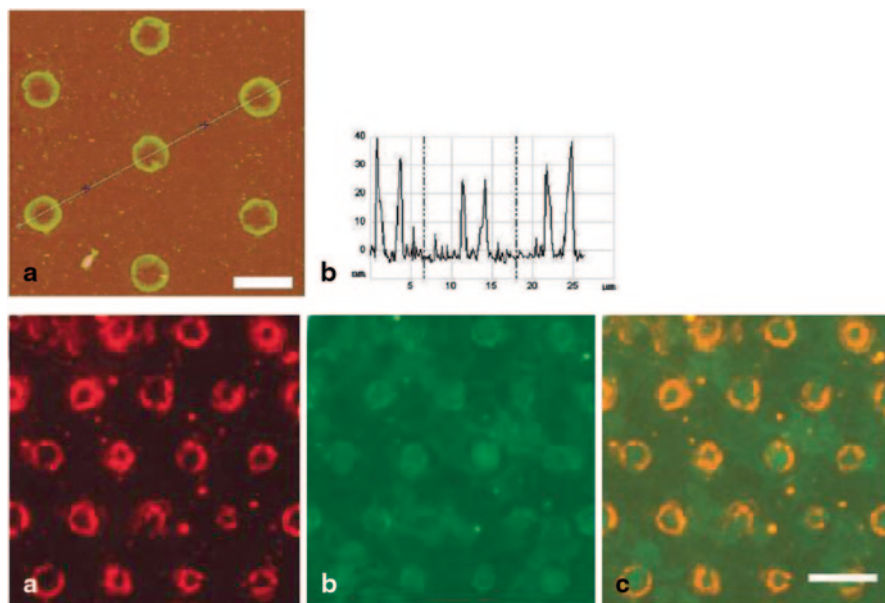


Fig. 12.15 *Top row*: The AFM topography images of the protein annuli hexagonal array. *Bottom row*: Fluorescence microscopy images of a hexagonal annulus structure. **a** Anti-GFP Dy Light 549-labelled antibodies (Ab1.3). **b** GFP bound to Ab1.3. **c** Overlay of **a** and **b**. The scale bar is 20 μm [40]

area drying, which is the key step for the annulus shape formation; (e). removal of colloidal template by adhesive tape lift-off.

As shown by the AFM image of the proteins-assembled annulus, the ring structure is defined by the original contact area between the colloids and substrate. Therefore, the annuli array is a direct replica of the 2D hexagonal colloidal assembly. As depicted in Step D in the Scheme, as the final stage of protein solution drying process, the protein molecules are swept around the bottom of the spheres, as the capillary contact lines recede. Therefore, the size of the rings is defined by the colloidal particle size and the sphere-substrate contact area. AFM imaging also reveals that the height of the annuli is in the range of 25–40 nm, which corresponds to two to three layers of antibodies. Fluorescence microscopy analysis displayed in Fig. 12.15 bottom row shows the red annuli arrays for anti-GFP DyLight 549-labelled antibodies, and their retained specific binding affinity to GFP.

Wolf and Li's study showed that the evaporation rate is a critical factor in the formation of the antibody annuli; accelerated drying by providing a vacuumed environment or elevated temperature did not result in similar ordered ring structures. It was also found that both the solvent and the antibody concentration play important roles on protein arrangement in the drying process. It appeared that the addition of surfactant Tween20 is also crucial for the protein sweeping process to take place, otherwise, the proteins would simply form connected network covering areas which

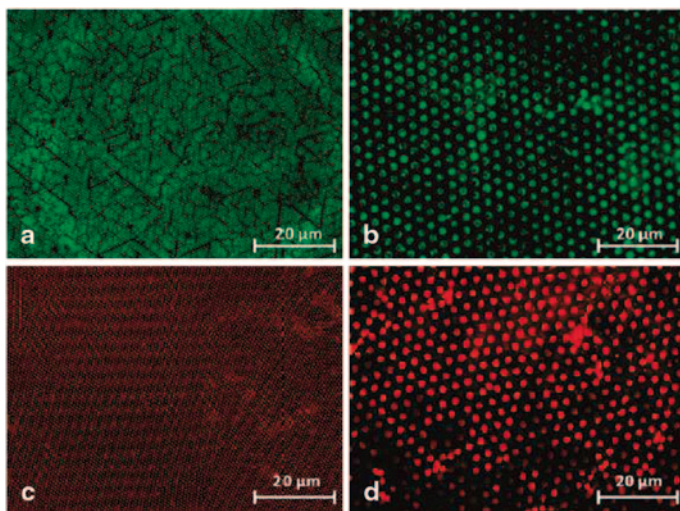


Fig. 12.16 FM images demonstrate a specific adsorption of R-BSA on unmodified glass regions on different chemical patterns generated from: **a** 2 μm COOH-PS/200 nm NH₂-PS, scale bar =20 μm , **b** 5 μm plain-SiO₂/500 nm NH₂-PS ($j_5 \mu\text{m} = 1.4 \times 10^{-3}$ and $j_{500 \text{ nm}} = 1.1 \times 10^{-4}$), scale bar =20 μm . FM images showing fluorescent signals from dislike Au features on the glass substrate produced from BCA masks: **c** 2 μm plain-SiO₂/200 nm NH₂-PS, scale bar =20 μm ; **d** 5 μm plain-SiO₂/500 nm NH₂-PS, Scale bar=20 μm [27]

are not protected by the colloidal particles. Two possible reasons were attributed to this observation: (a). the protein mobility on glass surface may be increased by the presence of the surfactant; (b). the meniscus between the template spheres break earlier in the presence of surfactants due to reduced surface tension, facilitating the formation of disconnected ring structure. In addition, there is a working range for the protein concentration; too low or too high would result in no pattern formation or too high a ‘protein blanket’ over the non-protected surface.

As the study has demonstrated, such protein annuli array patterns are robust; they did not show any sign of degradation after rewetting, for instance, by the aqueous secondary antibody solution. The authors concluded that the proteins are strongly bound to the glass substrate and connected to each other simply by the drying procedure while retaining their bioactivity. The subject of protein folding during drying in air itself is highly complex, which deserves particular attention in protein patterning. The annulus shape of this protein pattern provides a 3D extension based on the 2D colloidal templating, which is envisaged to have a significant advantage in antigen and cell binding due to the entrapment effect.

12.3.1.3 Patterning Based on 2D Binary Colloidal Assembly

As laid out in earlier section, variations in size and spacing of colloidal particles in the binary colloidal assembly (BCA) allow for tunable chemical patterns to be formed. Singh et al. [27] have demonstrated that arrays of disc-like patterns, with disc diameter in the range of hundreds of nanometres to a few μm and lateral distance ranging on the same order, can be formed by using BCAs comprised of large and small particles as masks for Au sputtering. The method is simple and versatile.

Singh et al. [27] further demonstrated that the patterns were capable of allowing selective protein adsorption to the unmodified regions. The patterns formed by Au sputtering for 10 min using a BCA mask were exposed to tetramethylrhodamine-labelled bovine serum albumin (R-BSA). The patterns were then examined by fluorescent microscopy (FM) as shown in Fig. 12.16, which shows that the fluorescent signals are mostly due to R-BSA specifically adsorbing onto the unmodified SiO_2 regions within the patterned surface.

12.3.2 3D Protein Templating

There are at least two modes in 3D protein patterning via colloidal templating. The first type is based on 3D colloidal crystal structure, which provides a homogenous distribution of proteins in a 3D ordered porous network, whereas the second type is related to transforming colloidal particles into vehicles for proteins, which is fundamental to a range of biomedical applications.

12.3.2.1 Protein Patterning via 3D Colloidal Crystals

The macroporous network derived from colloidal templates attracts particular interest from a chemo/biosensing perspective, due to its combinatorial advantages: in addition to the enormous surface area provided by the porous structure for immobilizing the target analytes, the ordered porous structure can also act as the transducer that converts the binding event into an optical signal, following Bragg's equation for the adsorption maxima [5].

For immobilizing proteins in the porous network, various strategies have been developed. Depending on the chemistry nature of the porous network, different protein linking molecules/elements can be first introduced on the surface via silane chemistry [42], or esterification reaction [43], or incorporation of protein-binding metals [44]. Protein functionalized 3D inverse opals have been demonstrated as effective label-free antigen-antibody sensor [44, 45].

Xia and coworkers [46, 47] have employed surface-functionalized inverse opals as a novel class of scaffolds with uniform and controllable pore sizes for tissue engineering to provide better nutrient transport, a uniform cell distribution and an adjustable microenvironment for cell differentiation. In a recent study [46], they reported that a truly 3D microenvironment can be created inside a pore by fur-

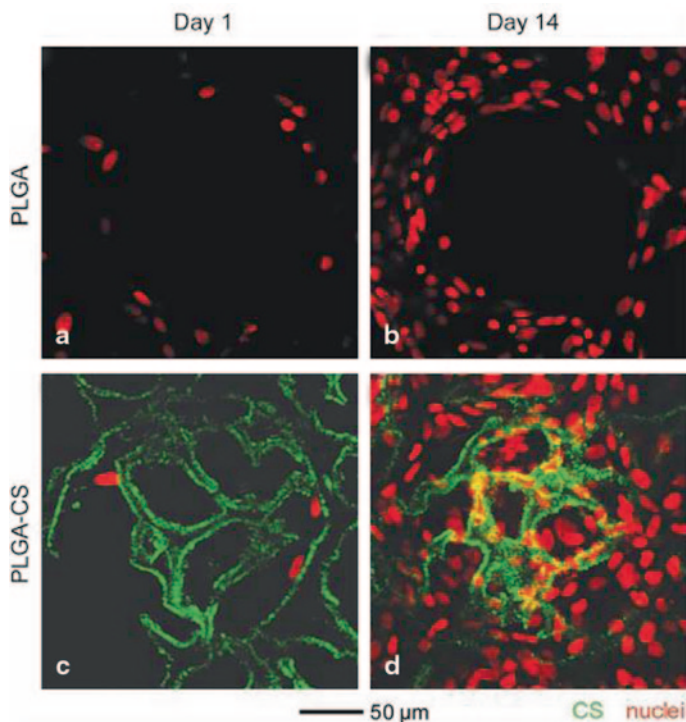


Fig. 12.17 Confocal fluorescence micrographs showing cell proliferation in the scaffolds. The focal depth was $\sim 50 \mu\text{m}$ from the surface of the scaffold, and the layer thickness was $\sim 5 \mu\text{m}$. **a**, **b** The cells only proliferated along the walls of the pores in a PLGA scaffold and still could not completely fill the void space of a pore after 14 d of culture. **c**, **d** The cells were able to attach to the microstructures inside the pores of a PLGA-chitosan scaffold and could also populate the centre region of the pore. Here, CS was prelabelled with fluorescein isothiocyanate and nuclei were stained with PI [46]

ther functionalizing the as-prepared inverse opal scaffold with chitosan by freeze-drying. The resultant inverse opal scaffold with hierarchically structured pores enhanced both cell proliferation and tissue infiltration. It can be envisioned that the 3D microenvironment can be further improved by introducing patterned protein on pore surfaces to mimic the *in vivo* cell environment (Fig. 12.17).

12.3.2.2 3D Protein Patterning via Colloidal Templating

3D protein assemblies can be prepared by repeated deposition of biotin–protein conjugate pairs operating as binding mediators between layers, or self-assembly techniques involving hybrid protein–polyelectrolyte multilayer films and protein–colloid multilayers. One of the earlier studies into the use of colloidal particles for controlled fabrication of protein multilayers was conducted by Caruso and Möh-

wald [48]. In this study, a layer-by-layer self-assembly strategy was employed to construct protein-shell structures onto colloids. To facilitate protein adsorption, polyelectrolytes were placed in suspension with PS particles to produce coated polyelectrolyte-colloid particles. Protein layers were then constructed by alternating adsorption of the polyelectrolyte-coated PS particles with protein solution and with polyelectrolyte solution of opposite charge to previous layers thereby facilitating film growth by exploiting electrostatic interactions. After each deposition of either protein or polyelectrolyte, samples were centrifuged and washed to remove supernatant. Using this method, Caruso and Möhwald [48] succeeded in creating multilayer protein films comprising of fluorescein isothiocyanate-labelled bovine serum albumin (FITC-BSA) and immunoglobulin G (IgG). Operating on the same basic strategy and principles as Caruso and Möhwald [48], Caruso and Schüler [49] formed glucose oxidase and horseradish peroxidase enzyme multilayers on polyelectrolyte-coated PS colloidal particles.

12.4 Conclusions

Chemically patterned surfaces with multiple feature length scales for selective immobilization of biomolecules are instrumental for the development of biosensors and bioanalytics, drug screening, tissue engineering and fundamental studies of cell biology. Colloidal templating based on self-assembly of colloidal particles provides an important technique that can create a feature size ranging from tens of nanometres to several μm in either 2D array or ordered 3D spatial configuration. As illustrated by the examples presented in this chapter, colloidal self-assembly can be tuned in various ways to create different types of patterns. Moreover, colloidal templating has significant advantages in that it does not require elaborate equipment, and being an intrinsic parallel process, the technique can be easily integrated with main stream materials deposition facilities such as sputtering/evaporation, chemical vapour deposition, reactive ion etching, plasma treatment, spotting and inkjet printing. Therefore, it is a promising technique in the development of proteometrics and bioanalysis.

References

1. Deckman, H.W. and J.H. Dunsmuir, *NATURAL LITHOGRAPHY*. Applied Physics Letters, 1982. **41**(4): p. 377–379.
2. Gates, B., S.H. Park, and Y.N. Xia, *Tuning the photonic bandgap properties of crystalline arrays of polystyrene beads by annealing at elevated temperatures*. Advanced Materials, 2000. **12**(9): p. 653-+.
3. Holtz, J.H. and S.A. Asher, *Polymerized colloidal crystal hydrogel films as intelligent chemical sensing materials*. Nature, 1997. **389**(6653): p. 829–832.
4. Kulinowski, K.M., et al., *Porous metals from colloidal templates*. Advanced Materials, 2000. **12**(11): p. 833–838.

5. Li, Q., et al., *Porous Networks Through Colloidal Templates*. Topics in Current Chemistry, 2009. **287**: p. 135–180.
6. Marquez, M. and B.P. Grady, *The use of surface tension to predict the formation of 2D arrays of latex spheres formed via the Langmuir-Blodgett-like technique*. Langmuir, 2004. **20**(25): p. 10998–11004.
7. Wright, J.P., et al., *Ultraflat ternary nanopatterns fabricated using colloidal lithography*. Advanced Materials, 2006. **18**(4): p. 421- +.
8. Trujillo, N.J., S.H. Baxamusa, and K.K. Gleason, *Grafted Functional Polymer Nanostructures Patterned Bottom-Up by Colloidal Lithography and Initiated Chemical Vapor Deposition (iCVD)*. Chemistry of Materials, 2009. **21**(4): p. 742–750.
9. Choi, D.G., et al., *Colloidal lithographic nanopatterning via reactive ion etching*. Journal of the American Chemical Society, 2004. **126**(22): p. 7019–7025.
10. Singh, G., et al., *Highly Ordered Nanometer-Scale Chemical and Protein Patterns by Binary Colloidal Crystal Lithography Combined with Plasma Polymerization*. Advanced Functional Materials, 2011. **21**(3): p. 540–546.
11. Hou, J., et al., *Bio-Inspired Photonic-Crystal Microchip for Fluorescent Ultratrace Detection*. Angewandte Chemie-International Edition, 2014. **53**(23): p. 5791–5795.
12. Yi, D.K., et al., *Colloid Lithography-Induced Polydimethylsiloxane Microstructures and their Application to Cell Patterning*. Biotechnology Letters, 2006. **28**(3): p. 169–173.
13. Wang, Y.C., et al., *Stretched inverse opal colloid crystal substrates-induced orientation of fibroblast*. Biomedical Materials, 2010. **5**: p. 035011.
14. Gleason, N.J., et al., *Patterning Proteins and Cells Using Two-Dimensional Arrays of Colloids*. Langmuir, 2003. **19**(3): p. 513–518.
15. Curtis, A. and M. Riehle, *Tissue engineering: the biophysical background*. Physics in Medicine and Biology, 2001. **46**(4): p. R47.
16. Jonas, U., et al., *Colloidal assemblies on patterned silane layers*. Proceedings of the National Academy of Sciences of the United States of America, 2002. **99**(8): p. 5034–5039.
17. Yang, P.D., et al., *Hierarchically ordered oxides*. Science, 1998. **282**(5397): p. 2244–2246.
18. Ekblad, T. and B. Liedberg, *Protein adsorption and surface patterning*. Current Opinion in Colloid & Interface Science, 2010. **15**(6): p. 499–509.
19. Li, Q., et al., *The forces at work in colloidal self-assembly: a review on fundamental interactions between colloidal particles*. Asia-Pacific Journal of Chemical Engineering, 2008. **3**(3): p. 255–268.
20. Dimitrov, A.S. and K. Nagayama, *Continuous Convective Assembling of Fine Particles into Two-Dimensional Arrays on Solid Surfaces*. Langmuir, 1996. **12**(5): p. 1303–1311.
21. Yoshimura, H., et al., *Two-dimensional crystallization*. Nature, 1993. **361**(6407): p. 26–26.
22. Wang, D.Y. and H. Mohwald, *Rapid fabrication of binary colloidal crystals by stepwise spin-coating*. Advanced Materials, 2004. **16**(3): p. 244- +.
23. Retsch, M., et al., *Fabrication of Large-Area, Transferable Colloidal Monolayers Utilizing Self-Assembly at the Air/Water Interface*. Macromolecular Chemistry and Physics, 2009. **210**(3–4): p. 230–241.
24. Zhou, Z., et al., *Fabrication of binary colloidal crystals and non-close-packed structures by a sequential self-assembly method*. Langmuir, 2007. **23**(3): p. 1473–1477.
25. Vogel, N., et al., *Plasmon Hybridization in Stacked Double Crescents Arrays Fabricated by Colloidal Lithography*. Nano Letters, 2011. **11**(2): p. 446–454.
26. Vogel, N., et al., *Laterally Patterned Ultraflat Surfaces*. Small, 2009. **5**(7): p. 821–825.
27. Singh, G., et al., *Large-area protein patterns generated by ordered binary colloidal assemblies as templates*. ACS nano 2011. **5**(5): p. 3542.
28. Denkov, N.D., et al., *MECHANISM OF FORMATION OF 2-DIMENSIONAL CRYSTALS FROM LATEX-PARTICLES ON SUBSTRATES*. Langmuir, 1992. **8**(12): p. 3183–3190.
29. Ramiro-Manzano, F., et al., *Colloidal Crystal Thin Films Grown into Corrugated Surface Templates*. Langmuir, 2010. **26**(7): p. 4559–4562.
30. Xia, Y.N., et al., *Monodispersed colloidal spheres: Old materials with new applications*. Advanced Materials, 2000. **12**(10): p. 693–713.

31. Yan, Q.F., Z.C. Zhou, and X.S. Zhao, *Inward-growing self-assembly of colloidal crystal films on horizontal substrates*. Langmuir, 2005. **21**(7): p. 3158–3164.
32. Li, Q., et al., *Porous Networks Through Colloidal Templates*, in *Templates in Chemistry Iii*, P. Broekmann, K.H. Dotz, and C.A. Schalley, Editors. 2009, Springer-Verlag Berlin: Berlin. p. 135–180.
33. Li, Q. and E. Eftekhari, *Hierarchically Ordered Colloid Crystals: Fabrication, Structures, and Functions*, in *Nanostructures: Properties, Production Methods and Applications*, Y. Dong, Editor. 2013, Nova Science Publishers, Inc.: Hauppauge, NY, USA. p. 169–181.
34. Lau, K.H.A., et al., *Self-assembly of Protein Nanoarrays on Block Copolymer Templates*. Advanced Functional Materials, 2008. **18**(20): p. 3148–3157.
35. Li, Q., et al., *The Effect of Fluid Flow on Selective Protein Adsorption on Polystyrene-block-Poly(methyl methacrylate) Copolymers*. Langmuir, 2009. **25**(20): p. 12144–12150.
36. Fu, J., et al., *3D Hierarchically Ordered Composite Block Copolymer Hollow Sphere Arrays by Solution Wetting*. Langmuir, 2010. **26**(14): p. 12336–12341.
37. Wang, J., et al., *Structural and optical characterization of 3D binary colloidal crystal and inverse opal films prepared by direct co-deposition*. Journal of Materials Chemistry, 2008. **18**(9): p. 981.
38. Wang, L., et al., *Binary Colloidal Crystals Fabricated with a Horizontal Deposition Method*. Langmuir, 2009. **25**(12): p. 6753–6759.
39. Wang, J., et al., *Preparation of multilayered trimodal colloid crystals and binary inverse opals*. Journal of the American Chemical Society, 2006. **128**(49): p. 15606–15607.
40. Wolf, C. and Q. Li, *Tunable Two-Dimensional Array Patterning of Antibody Annuli through Microsphere Templating*. Langmuir, 2010. **26**(14): p. 12068–12074.
41. Vakarelski, I.U., et al., *Assembly of Gold Nanoparticles into Microwire Networks Induced by Drying Liquid Bridges*. Physical Review Letters, 2009. **102**(5): p. 4.
42. del Campo, A., et al., *Surface modification with orthogonal photosensitive silanes for sequential chemical lithography and site-selective particle deposition*. Angewandte Chemie-International Edition, 2005. **44**(30): p. 4707–4712.
43. Cassagneau, T. and F. Caruso, *Inverse opals for optical affinity biosensing*. Advanced Materials, 2002. **14**: p. 1629–1633.
44. Qian, W.P., et al., *Three-dimensionally ordered macroporous polymer materials: An approach for biosensor applications*. Langmuir, 2002. **18**(11): p. 4526–4529.
45. Choi, E., et al., *Label-free specific detection of immunoglobulin G antibody using nanoporous hydrogel photonic crystals*. Sensors and Actuators B-Chemical, 2013. **180**: p. 107–113.
46. Zhang, Y., S.W. Choi, and Y.N. Xia, *Modifying the Pores of an Inverse Opal Scaffold With Chitosan Microstructures for Truly Three-Dimensional Cell Culture*. Macromolecular Rapid Communications, 2012. **33**(4): p. 296–301.
47. Zhang, Y.S., S.W. Choi, and Y.N. Xia, *Inverse opal scaffolds for applications in regenerative medicine*. Soft Matter, 2013. **9**(41): p. 9747–9754.
48. Caruso, F. and H. Möhwald, *Protein Multilayer Formation on Colloids through a Step-wise Self-Assembly Technique*. Journal of the American Chemical Society, 1999. **121**(25): p. 6039–6046.
49. Caruso, F. and C. Schüller, *Enzyme Multilayers on Colloid Particles: Assembly, Stability, and Enzymatic Activity*. Langmuir, 2000. **16**(24): p. 9595–9603.